Lab on a Chip

Cite this: *Lab Chip*, 2011, **11**, 1118

www.rsc.org/loc

PAPER

Continuous separation of breast cancer cells from blood samples using multi-orifice flow fractionation (MOFF) and dielectrophoresis (DEP)

Hui-Sung Moon,†[a] Kiho Kwon,†[a] Seung-Il Kim,[b] Hyunju Han,[b] Joohyuk Sohn,[b] Soohyeon Lee[b] and Hyo-Il Jung*[a]

Received 27th August 2010, Accepted 6th January 2011
DOI: 10.1039/c0lc00345j

Circulating tumor cells (CTCs) are highly correlated with the invasive behavior of cancer, so their isolations and quantifications are important for biomedical applications such as cancer prognosis and measuring the responses to drug treatments. In this paper, we present the development of a microfluidic device for the separation of CTCs from blood cells based on the physical properties of cells. For use as a CTC model, we successfully separated human breast cancer cells (MCF-7) from a spiked blood cell sample by combining multi-orifice flow fractionation (MOFF) and dielectrophoretic (DEP) cell separation technique. Hydrodynamic separation takes advantage of the massive and high-throughput filtration of blood cells as it can accommodate a very high flow rate. DEP separation plays a role in precise post-processing to enhance the efficiency of the separation. The serial combination of these two different sorting techniques enabled high-speed continuous flow-through separation without labeling. We observed up to a 162-fold increase in MCF-7 cells at a 126 μL min^{-1} flow rate. Red and white blood cells were efficiently removed with separation efficiencies of 99.24% and 94.23% respectively. Therefore, we suggest that our system could be used for separation and detection of CTCs from blood cells for biomedical applications.

Introduction

It is generally accepted that circulating tumor cells (CTCs) in the peripheral blood of cancer patients are highly correlated with the "invasive behaviors" of a proportion of cancer cells.[1,2] The precise measurement or isolation of CTCs can serve as a powerful tool for cancer prognosis, diagnosis of minimal residual disease, assessment of tumor sensitivity to anticancer drugs, and personalization of anticancer therapy.[3,4] Several microfluidic devices have recently been reported for the detection and isolation of CTCs. For example, microchips containing microposts coated with EpCAM antibody have been used to identify CTCs through immunocapture.[5] A high aspect ratio microchannel was also developed to capture CTCs using the same antibody to enhance the throughput.[6] Both of these approaches effectively captured rare CTCs in a large sample volume, which enables the detection of CTCs but does not allow for the retrieval of live cells for downstream analysis. Moreover, it was recently reported that some tumor cells express low or no EpCAM, resulting in a limited binding efficiency.[7] Dielectrophoresis can also be used to separate CTCs and blood cells.[8] It can position the target cells and other cells in different locations between electrodes without the need for a labeling process. However, collection of the separated cells remains very difficult. A mechanical sieve can isolate CTCs based on size differences.[9] Although it is simple and easy to use, a high concentration of cells will create a blockage, and harvesting the captured cells is also inconvenient. To collect and analyze CTCs, label-free and continuous flow-through separation is needed. Magnetophoretic removal of red blood cells using their intrinsic paramagnetic properties is a good candidate method for CTCs isolation[10] if white blood cells can be separated with CTCs. The main challenge in developing a CTC detection or separation chip is the extremely low concentration of CTCs in blood (as few as one cell per 10^9 hematologic cells or 0 to 1 cell per 1 mL).[10–14] When sampling rare events in a large population, three important metrics must be assessed: (1) throughput, the number of cells sorted per unit time; (2) recovery, an indicator of the fraction of target cells collected from the input sample; and (3) purity, which depends on the number of "interfering" cells excluded from the analysis.[15] In addition, it is important to provide highly efficient quantification of the number of enriched cells.[6]

Hydrodynamic sorting, a separation or focusing technique based on inertial microfluidics,[16] is gaining recognition.[17,18] This process enables continuous and high throughput separation of different particles without the application of external forces. In a previous study, we introduced a novel hydrodynamic method for size-based particle separation,[19] multi-orifice flow

[a]*School of Mechanical Engineering, Yonsei University, 262 Seongsan-no Seodaemun-gu, Seoul, 120-749, South Korea. E-mail: uridle7@yonsei.ac.kr; Fax: +82-(0)2-312-2159; Tel: +82-(0)2-2123-5814*
[b]*College of Medicine, Yonsei University, 250 Seongsan-no Seodaemun-gu, Seoul, 120-752, South Korea*
† These authors contributed equally to this paper.

fractionation (MOFF), in which the microparticle is moved laterally due to hydrodynamic inertial forces created by a multi-orifice structure.[20] The extent of lateral movement varies according to particle size and polymer microspheres can be concentrated at different lateral positions in a microchannel. This technique is advantageous for CTC separation because of its simple experimental set up and much higher operational flow rate (100–300 μL min^{-1}) compared to those of other microfluidic separators. However, the output purity of this device is not sufficient for CTC separations necessitating the introduction of a secondary purification modality.

Dielectrophoresis (DEP), the translational motion of charge-neutral matter caused by polarization effects in non-uniform electric fields,[21] is a recently emerging technique capable of rapid separation of cells in microfluidic devices due to the significant contactless cellular forces created by low voltages in the absence of modification or labeling.[22] We previously reported a DEP cell separator with a novel curved electrode design to isolate bacterial cells from environmental particles.[23] DEP cell separators can have a relatively high output purity due to the specificity of the dielectric phenotype of a particle. With a relatively slow flow rate, the DEP separator has the best performance. If the flow rate increases, purity decreases because the weak DEP forces have less of a chance to affect the cells. Therefore, in this study we decoupled the trade-off between speed and sensitivity by integrating the two independent techniques of hydrodynamic separation (primary) and DEP separation (secondary) for CTC separation. The resultant integrated system was capable of fast CTC separation at a high flow rate (126 μL min^{-1}) with high efficiency (~99.24%) and without labeling. The hydrodynamic separation performed massive and fast filtration, and DEP separation played a role in precise post-processing. Such a serial combination of various separation methods is a good strategy for increasing separation efficiency, as demonstrated by other recent attempts. Dielectrophoretic separation has been combined with magnetic trap techniques[24] and a label-free lateral magneto-dielectrophoretic microseparator[25] has been proposed. Also a two-step process composed of multi-orifice microchannel and spiral microchannel has been presented.[26] Here, we demonstrated that our microfluidic device continuously separated MCF-7 cells from blood cells. MCF-7s are malignant human breast cancer epithelial cells and known CTCs.[27] We believe that our device will contribute to the study of breast cancer, the most common cancer in women.[28]

Materials and methods

Device design

The microfluidic device consists of serially integrated MOFF and DEP separators (Fig. 1a). Once samples are introduced through the inlet, most of the blood cells are separated *via* MOFF and extracted through outlet I. Breast cancer cells (MCF-7s) with residual blood cells (not fully separated) proceed to the DEP separator. Finally, the cancer cells exit through outlet II and residual blood cells through outlet III.

The MOFF component is composed of one inlet, a filter, a multi-orifice segment, a fraction segment and two wide outlets. The designed depth of the microchannel is 60 μm. The

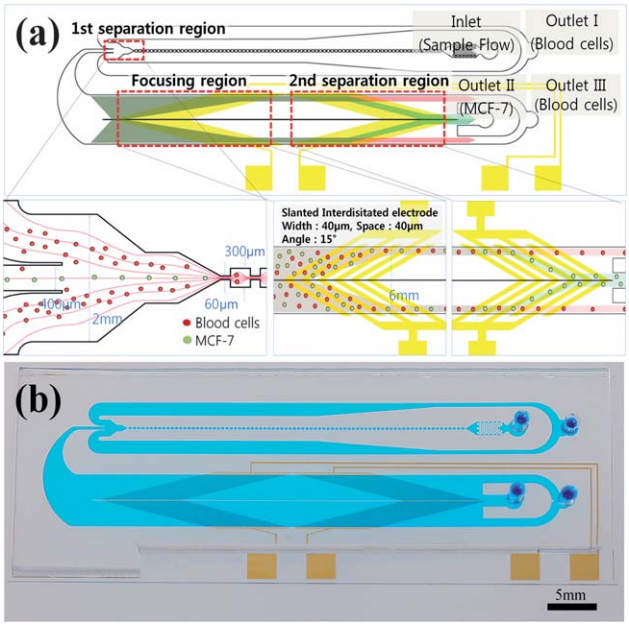

Fig. 1 (a) Schematic diagram of our microfluidic device for cancer cell separation using MOFF and DEP. In the first separation region, the relatively larger MCF-7 cells and a few blood cells pass through the center channel and enter the DEP channel, after which most blood cells exit through outlet I. In the focusing region, all cells experience a positive DEP force and then align along both sides of the channel. Finally, the second separation region selectively isolates MCF-7 cells *via* DEP. (b) Photographic image of the fabricated device.

multi-orifice segment consists of an alternating series of contraction channels and expansion chambers. The total length of the multi-orifice segment is about 36 mm and contains 80 repeated contraction/expansion elements. We previously found that the particle distribution was stabilized beyond the 80th orifice and that particle behavior could be correlated with the particle Reynolds number (Re_p),[19] a dimensionless number that provides a measure of the ratio of inertial forces to viscous forces, characterizing the motion of fluid in the microchannel. In addition, the size fraction of particles and channels is considered Re_p. We described the fluid dynamic phenomenon of particles flowing *via* a multi-orifice channel using Re_p, which is expressed as

$$Re_p = Re_c \frac{d^2}{D_h^2} = \frac{\rho U_m d^2}{\mu D_h} \quad (1)$$

where D_h is the hydraulic diameter of the channel, U_m is the maximum flow velocity in the channel, ρ is the density of the fluid, and μ is the dynamic viscosity of the fluid.

Our previous experimental results were used to select the dimension of the multi-orifice channel for separating MCF-7s and blood cells. Particles with a 15 μm diameter have a tendency to focus at the middle of the channel, in the range of 4.43–10.1 Re_p. In the case of 7 μm particles, we observed focusing along both sides of the channel walls within the Re_p range of 0.55 to 1.38.[19] In order to achieve size-based particle separation, these two conditions have to be satisfied simultaneously. In this study, we chose the particle sizes of 8 μm and 20 μm, similar to the average sizes of red blood cells and MCF-7s respectively, to determine the dimensions of the MOFF channel for MCF-7

isolation. Even though there are various types of leukocytes, the average sizes of neutrophils and lymphocytes, which account for most leukocytes (>75%), are about 8 μm.

We plotted the separation flow rate zones of these two different sizes of particles according to the three different dimensions of the orifice channel (width of contraction region = 45 μm, 60 μm and 75 μm) (Fig. 2). The Re_p of the larger particles (20 μm; solid line) should be between 4.43 and 10.1 to allow for focusing in the centerline of the channel. At the same time, the smaller particles (8 μm; dashed line) should have an Re_p value between 0.55 and 1.38 to bifurcate to both sides of the channel. The range of Re_c that satisfies both conditions was marked according to the width of the contraction channel in Fig. 2, allowing us to obtain the proper working conditions of the MOFF channel to isolate the MCF-7 from blood cells.

We chose a contraction channel dimension of 60 μm for MCF-7 separation (Fig. 2b). When the channel was smaller than 60 μm, the working flow rate was lowered, although the range of Re_c allowing separation could not be narrowed (Fig. 2a). Stable performance cannot be achieved in an excessively narrow range of separation. In addition, we experienced an intermittent clogging problem with a channel width of 45 μm. On the other hand, when the channel was wider than 60 μm, the working flow rate and the separable zone both increased (Fig. 2c). However, channel expansion is constrained by the possibility of cell damage due to high shear stress. The dimensions of the contraction channels are 60 μm in width and 150 μm in length, while those of the expansion chambers are 300 μm in both width and length. At the end of the multi-orifice segment, the main channel is divided into smaller larger cell outlets. The central channel is for the larger cells (MCF-7s), with a 400 μm channel width and a link to outlets II and III *via* DEP separation. The other two side channels, with widths of 760 μm, collect the smaller cells (blood cells) and release them through outlet I. Each branch channel portion was determined based on the positions of cells.

The DEP separator starts with a widening connecting channel (Fig. 1a). Since only approximately one-half of the injected sample volume proceeds to the widened channel, the flow velocity can be significantly decreased (×1/200) to be suitable for DEP separation. The inside wall (50 μm width) splits the DEP channel into two symmetrical channels and prevents the collapse of the PDMS microchannel, which has a low aspect ratio (0.01). The channel for DEP separation is 6000 μm in width (2975 + 50 + 2975 μm) and 30 mm in length. Due to the absence of sheath flow, all the cells are directed to the side wall by the first set of DEP electrodes. At the second DEP electrodes, MCF-7 cells migrate to the center of the channel, while blood cells remain in the wall side stream due to the selective manipulation *via* DEP. The DEP electrodes are placed at the bottom of the channel and have an interdigitated structure that has 40 μm width and space and slanted at −15° and 15°. At the end of the DEP separation, the channel is split into two outlets, outlet II (center) for MCF-7 cells and outlet III (side) for blood cells.

Device fabrication

Soft-lithography was used to pattern the structures of the MOFF and DEP microchannels. Negative photoresist (SU-8 2050, MicroChem Corp., MA, USA) was spin-coated onto a four-inch silicon wafer and was subsequently subjected to several physicochemical processes, namely soft baking, UV light exposure, post-exposure baking, development, and hard baking. As a result, the SU-8 master template was formed on a silicon wafer with a thickness of 60 μm true to the proposed design. Next, for replica molding, an instant barrier was made by wrapping the master silicon wafer in aluminum foil. A 10 : 1 volumetric mixture of PDMS (Sylgard 184, Dow Corning Corp., MI, USA) and a curing agent were then poured onto the master wafer. After degassing the polymer mixture, the master wafer overspread with clear PDMS was cured on a hotplate at 75 °C for 90 minutes. After curing, the PDMS replica was removed from the master wafer and perforated at the channel inlet and outlet using a punch.

The DEP electrodes were fabricated on a four-inch glass wafer using a conventional photolithography process. Chromium and gold layers were deposited onto the wafer for electrodes with 200 Å and 3000 Å thickness, respectively, using sputter, and chromium was used as an adhesion layer. Photoresist (PR, AZ1512) was spin-coated to a 1 μm thickness, exposed under UV light and developed to define the electrode patterns. Gold etchant and hydrochloric acid (HCl) were used successively to define the electrodes, and acetone was used to remove the patterned PR. Lastly, the PDMS replica was assembled with fabricated electrode patterns onto the glass wafer after O_2 plasma treatment using a plasma generator (Cute-B Plasma, FEMTO Science Co.,

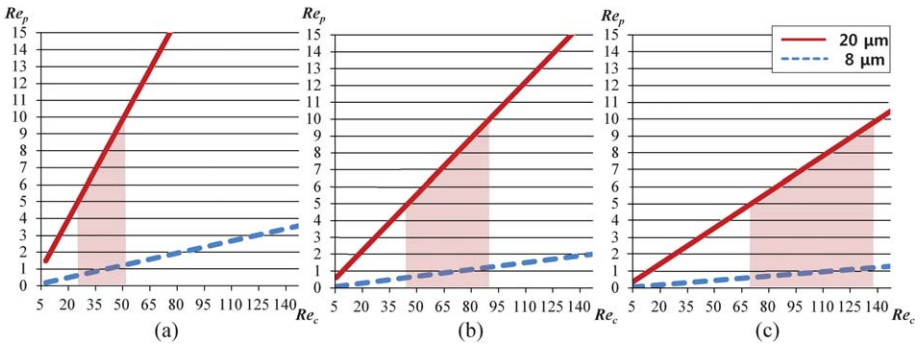

Fig. 2 Plot of separable flow rates expressed as channel Reynolds numbers (Re_c) according to varying contraction widths of the orifice channel: (a) 45 μm, (b) 60 μm, (c) 75 μm. The *y*-axis of the graph represents the particle Reynolds number.

Korea) and was stored overnight in an oven (75 °C) to ensure permanent bonding. Wires were attached to the electrodes using silver paste.

Sample preparation

Red blood cells (RBC), white blood cells (WBC) and MCF-7 breast carcinoma cells were used for the separation. Blood was drawn from healthy volunteers by phlebotomists. EDTA vacutainer tubes were used for blood collection. RBC and WBC were processed using density gradient separation. RBCs were briefly centrifuged from whole blood and diluted with working buffer. The working buffer was made of isotonic solution (8.5% sucrose + 0.3% dextrose, w/v) with phosphate buffered saline (PBS) to adjust the conductivity to 570 μS cm^{-1} and 1% bovine serum albumin (BSA) to reduce cell aggregation. WBCs were also centrifuged from the whole blood. Whole blood cells were first floated on Ficoll-Paque (GE Healthcare Bio-Sciences Corp., Uppsala, Sweden) and then centrifuged for 30 min at 1380 rpm, followed by careful isolation of the buffy coat. The isolated buffy coat was washed and diluted in PBS to remove residual Ficoll-Paque. The final step was an additional centrifugation for 10 min at 980 rpm to reduce contamination of the platelets. All blood samples were used within 6 h of collection.

We chose the MCF-7 breast carcinoma cell line as a model for circulating tumor cells (CTC). Cells were incubated under ordinary cell culture conditions. MCF-7 cells were cultured to 80% confluence in Dulbecco's modified Eagle's medium supplemented with high glucose and containing 1.5 g L^{-1} sodium bicarbonate ($NaHCO_3$), 15 mM HEPES buffer, and 10% fetal bovine serum (FBS). A 0.25% trypsin solution was prepared in 150 mM PBS and was used to harvest the MCF-7 cells. Cells were trypsinized, washed with PBS and resuspended in working buffer to the same concentration as those of the other blood cell samples. The initial concentrations of the suspended cells are listed in Table 1.

Experimental set up

A syringe pump (KDS200, KD Scientific Inc., MA, USA) was used to generate a continuous, stable micro flow over a wide flow rate range of 10 to 250 μL min^{-1}. The 2 mL syringe was connected to the inlet hole of the PDMS microchannel using silicone and aluminum tubes. Prior to performing each experiment, the system was degassed by filling with 70% ethanol and with PBS solution because the low polarity solvent wetted the hydrophobic PDMS surface more easily.[29] All samples used in this experiment contained 1% BSA to prevent cell adhesion.

Table 1 Specification of three different cells and the concentration of each sample

	Concentration ($\times 10^3$ μL^{-1})			
	RBC	WBC	MCF-7	Diameter/μm
Sample #1	10.0	—	—	6–9
Sample #2	—	1.0	—	6–10
Sample #3	—	—	1.0	16–24
Sample #4	10.0	0.01	0.01	—

An inverted optical microscope (I-70, Olympus Co., Japan) equipped with a halogen lamp was used to observe the moving cells in the microchannel which faced the objective lens. Images were captured using a high speed CCD camera (HotShot 1280; NAC Image Technology, CA, USA) every 100–125 μs. Data were analyzed with the image-processing programs Adobe Photoshop (Adobe Systems Inc., CA, USA) and ImageJ (NIH, MD, USA). An arbitrary/function generator (AGF3102, Tektronix, OR, USA) delivered AC potential to the DEP part of the device.

Separation efficiency

We evaluated the separation efficiency of our new device according to recovery and purity. The recovery is the percentage of particles successfully sorted from the total number of target particles within the initial fraction. Purity is defined as the number of target particles relative to the total number of particles in each outlet. We counted the numbers of cells after collection at each outlet. In the case of the mixed samples experiment, it was unclear how to distinguish blood cells from MCF-7 cells based on morphology alone; therefore, we used an immunocytochemical method. To count the cells in the mixed sample, we used three fluorescence markers; CD45 antibody was used to identify WBCs, DAPI for visualization of cell nuclei and EpCAM for MCF-7. The MCF-7 cells were defined as EpCAM+/DAPI+/CD45− and WBCs were identified as EpCAM−/DAPI+/CD45+. In addition, a cytospin centrifuge (Cytospin 3, Shandon Inc., PA, USA) was employed to smear the collected sample. A cytospin smear can reduce cell loss during the staining process and enhance the fluorescent image quality.[30] All of the separated samples were kept on ice and then 50 μL of each sample was cyto-centrifuged for 5 min at 2000 rpm. We used the immunocytochemical method mentioned above to calculate the recovery and the purity.

Results and discussion

Multi-orifice flow fractionation (MOFF)

We examined the specific ranges of the Reynolds numbers for which the cells would be concentrated laterally according to their sizes using a MOFF microchannel. The fluid flowing through a microchannel can be estimated using the channel Reynolds number (Re_c). We used a Re_c range from 30 to 90, based on the characteristic length of a contraction channel, and a flow rate of 54–162 μL min^{-1}. Fig. 3 shows the behaviors of three different cells in the separation region after flowing through the MOFF at various Reynolds numbers. We easily observed the behaviors of RBCs using the captured images. However, in order to obtain the photographic images of WBCs and MCF-7 cells, a post-image collection process was needed to increase the contrast with the background. We captured two images in a certain time interval from the same site in the channel to determine the exact concentration of cells. From these two images, all pixels with the same value were removed. As a result, high contrast images depicting the few cells that remained in the channel were obtained.

In the case of RBCs, cells were randomly spread out over a wide area at very low Re_c. With increasing Re_c, the cells

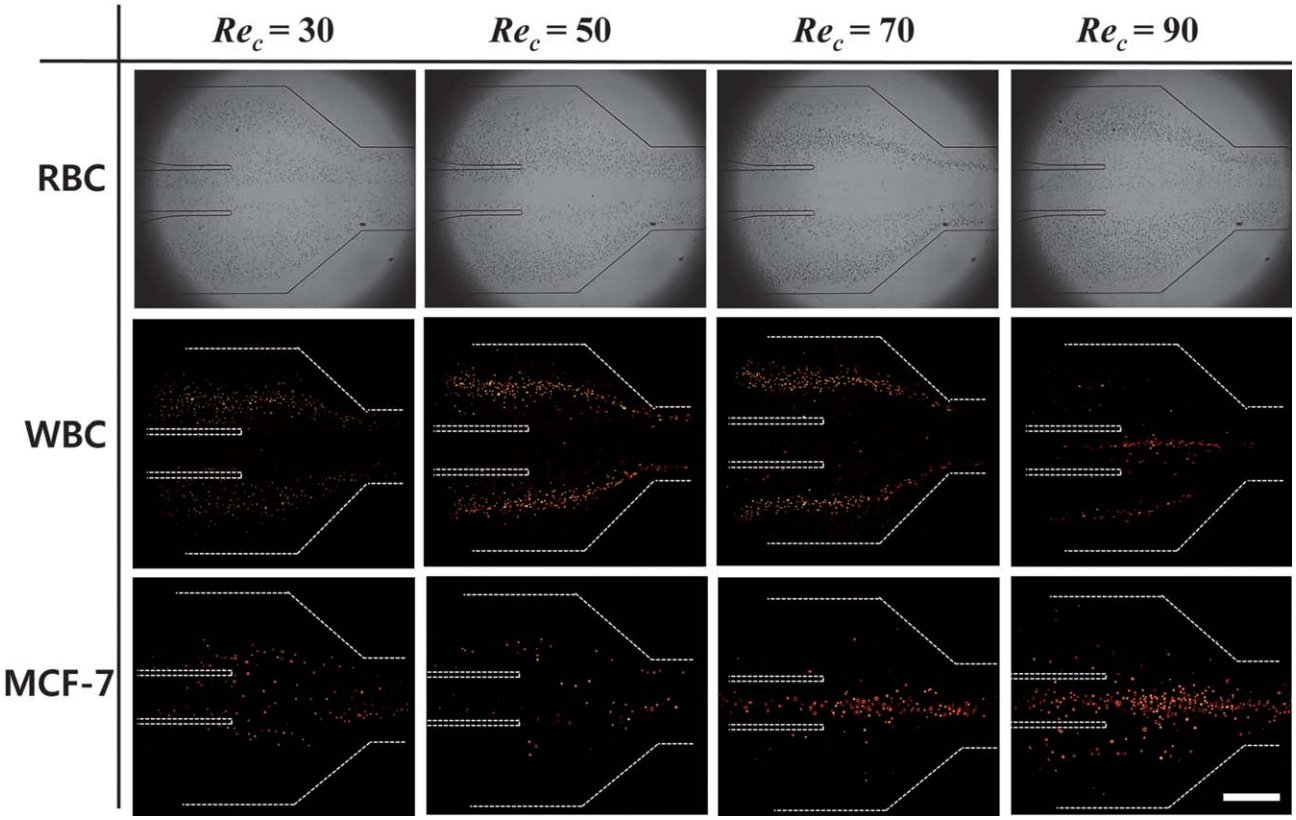

Fig. 3 Cell trajectories (RBC, WBC, and MCF-7) through the multi-orifice microchannel according to channel Reynolds number (Re_c). Cells were randomly spread out at low Re_c. With increasing Re_c, the distribution of cells stabilized at each equilibrium position based on size. When Re_c reached 70, the RBCs and WBCs separated into two positions and MCF-7 cells were focused in the middle of the channel. Scale bars represent 500 μm.

bifurcated at the end of the MOFF channel. At $Re_c = 30$, the RBCs started to bifurcate, and at $Re_c = 50$, the cells were clearly split into two groups. However, the particle streamline was still thick, with most of the cells, remaining in the middle channel. This explains the poor recovery of RBCs (58.43%). When the Re_c reached 70, the focused streamline of RBCs remained in the equilibrium position, resulting in 84.08% RBCs separation. As the Re_c increased to 90, the particle streamline increased in thickness, and the focused lines moved closer to the center of the channel. Based on these results, an Re_c of 70 was the best condition for focusing RBCs to the side wall.

The overall cell behavioral trend of WBCs was similar to that of RBCs. Since WBCs have larger diameters than do RBCs, they were more readily influenced by the inertial lift force from the MOFF channel. We observed two streamlines focused from 30 to 70 of Re_c, with the highest recovery achieved near 70 Re_c (81.18%). Therefore, the optimal flow condition was $Re_c = 70$, just as with the RBCs.

In the case of MCF-7 cells, recovery was high at both 30 and 70 Re_c. Even though MCF-7 cells flow along the channel at a low flow rate, the cells maintain a certain distance relative to the channel side wall. This is a result of a heavy wall effect-induced lift force, since the mean diameter of MCF-7 cells is 20 μm, relatively larger than other cell sizes and one-third of the channel width. When the Re_c reached 70, the streamlines were finely focused in the middle of the channel. As Re_c increased to greater than 90, the focused streamline of blood cells gradually approached the centerline, and the trajectory of MCF-7 cells gradually dispersed from the centerline. Thus, we considered the best separation condition for MCF-7 cells from blood cells to be $Re_c = 70$.

We next investigated the separation yield for a mixture of the three cell types (RBCs, WBCs, MCF-7) using the MOFF device. We found that the MOFF procedure could isolate 93.31% MCF-7 cells from the mixture of blood cells, while simultaneously removing 87.98% of RBCs and 61.94% of WBCs. The results of the separation efficiency using MOFF are summarized in terms of recovery and purity in Table 2.

Dielectrophoretic cell separation

After MOFF separation, the cells entered the DEP module, where they were subjected to dielectrophoretic forces created by a non-uniform electric field. In the focusing region (Fig. 4a), all of the cells experienced a positive DEP force toward the edge of the electrode in a perpendicular direction due to the pulling force. Due to the hydrodynamic force generated by fluid flow, all of the cells migrated in the y-direction along the slanted electrode at an applied voltage of 10 V_{pp}, 2 MHz. As the cells proceeded through the system, they were focused to the wall side (Fig. 4b) and into the separation region. Here, DEP electrodes produced a 10 V_{pp}, 900 kHz electric field which resulted in an attractive force sufficient only for the larger MCF-7 cells. Hence, only the MCF-7 cells were pulled upward along the electrodes, while blood cells

Table 2 Separation yields of RBC, WBC, and MCF-7 cells in the MOFF region depending on Reynolds number

Reynolds #			30			50			70			90		
Sample name			RBC	WBC	MCF-7	RBC	WBC	MCF-7	RBC	WBC	MCF-7	RBC	WBC	MCF-7
Independent samples	Recovery	Outlet II, III	38.36	44.50	89.33	14.28	39.58	64.20	15.92	18.82	88.83	70.85	59.15	73.52
		Outlet I	61.64	55.50	10.67	85.72	60.42	35.80	84.08	81.18	11.17	29.15	40.85	26.48
Mixed samples	Recovery	Outlet II, III	50.26	34.29	71.43	8.14	30.59	50.60	12.02	38.06	93.31	50.80	54.19	62.58
		Outlet I	49.74	65.71	28.57	91.59	69.41	49.40	87.98	61.94	6.69	49.20	45.81	37.42
	Purity	Outlet II, III	99.95	0.02	0.03	99.45	0.21	0.34	97.87	0.59	1.54	99.74	0.12	0.14
		Outlet I	99.95	0.03	0.01	99.93	0.04	0.03	99.85	0.13	0.02	99.81	0.10	0.09

passed straight through the channel (Fig. 4c). Since the DEP channel was split into two symmetrical channels by an inside wall, MCF-7 cells traversed the channel and exited through the inner outlet, outlet II (Fig. 5b). Meanwhile, blood cells moved along the side walls and exited through outlet III (Fig. 5a and c).

Usually, continuous DEP separators make use of negative rather than positive DEP since positive DEP causes unwanted adhesion between cells and electrodes and hinders the release of cells. Once the cells have adhered, the high-gradient electric field can affect their viabilities. To avoid this problem, we used AC voltage in 1 ms intervals of 0.5 ms of voltage followed by 0.5 ms of rest. During the resting period, the cells detached from the high electric field regions of the electrode edges and moved in the flow direction. When the voltage was reactivated, the cells were again attracted to the electrodes edges. This alternating process caused the cells to move in a direction parallel to the electrodes. A relatively fast flow velocity and the use of BSA may also help to prevent cells from sticking to the electrodes. The real part of the Clausius–Mossotti (CM) factor has a minimum value of −0.5 and maximum value of 1, with the sign of the factor indicating the type of force experienced by the particles. Therefore, we could use a positive DEP (positive CM factor) to our advantage because we can theoretically apply a DEP force that is greater than the negative DEP force.

Throughout the device, the separation efficiency of MCF-7 cells was 75.18%. This value was reduced by the accumulated MCF-7 losses after traveling through the two MOFF and DEP separation channels. In other words, the separated MCF-7 cells in the MOFF region experience a second separation *via* DEP, so the recovery is expected to further decrease. Nevertheless, MCF-7 cells were purified with an enrichment factor of 162. On the other hands, the separation efficiencies for the RBCs and WBCs were 99.24% and 94.23%, respectively. The blood cells content was relatively high compared to that of MCF-7 because of the loss of MCF-7 cells during serial separation. Since WBCs wary in diameter, ranging from 6–10 μm, and in cell types (*e.g.*, neutrophil, basophil, eosinophil, monocyte and lymphocyte), they do not display homogeneous physical properties. This inhomogeneity results in a slightly lower separation efficiency compared to that of RBC, as summarized in Table 3. Although the removal ratio of blood cells was very high, the purity of MCF-7 in the sample collected at outlet II was as low as 16.24%. Since the fraction of RBCs in the initial sample was extremely high, only 0.76% of unremoved RBC can significantly decrease the purity of MCF-7.

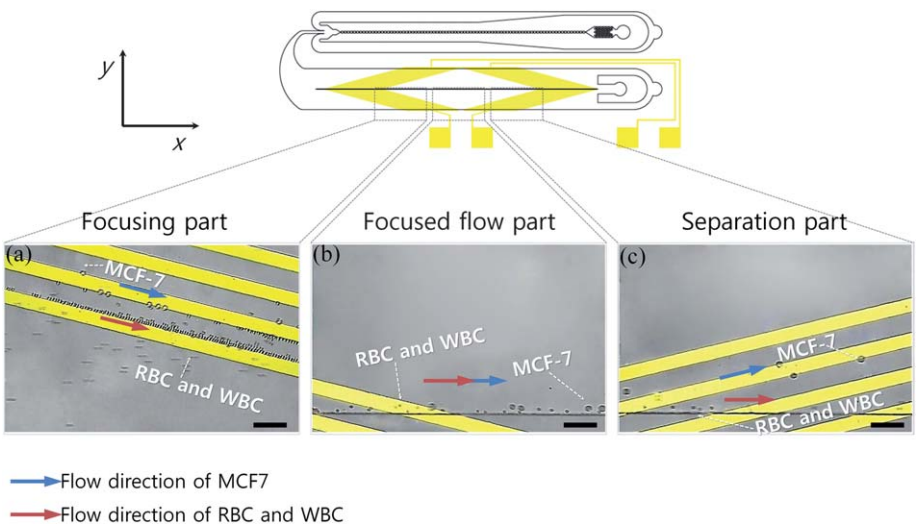

Fig. 4 Dielectrophoretic separation by cell type. The bigger cells are MCF-7 and the smaller ones are blood cells. (a) In the focusing region, by applying 2 MHz and 10 V_{pp}, all of the cells were forced to move along the wall due to the positive DEP. (b) All of the cells were focused to the side wall. (c) In the separation region, only MCF-7 cells moved upward to outlet II since the 10 V_{pp}, 900 kHz voltage pulled MCF-7s toward the edges of the electrodes. At the same time, blood cells were mostly unaffected by the DEP force and were directed to outlet III. Scale bars represent 80 μm. An upright microscope (BX-51, Olympus Co., Japan) was used for observation and image collection.

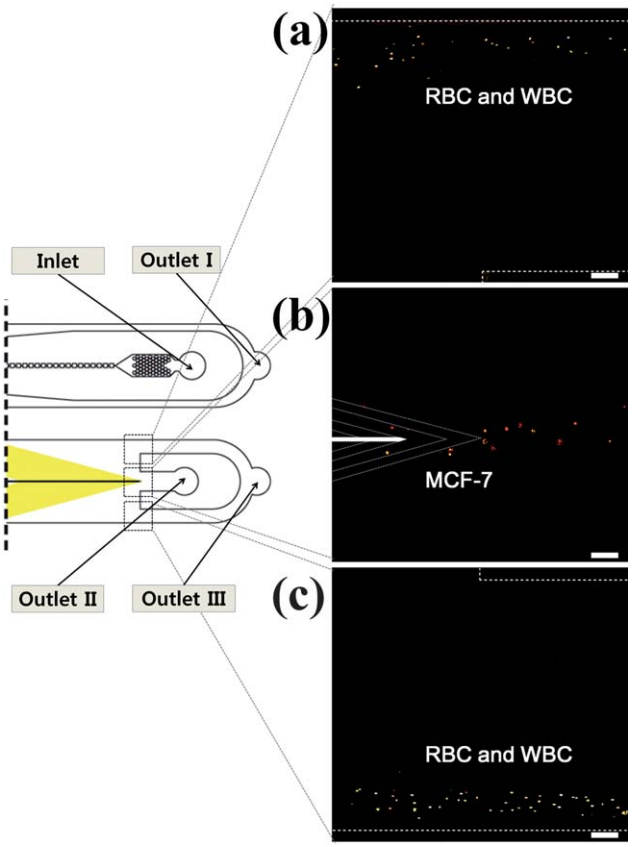

Fig. 5 Images taken in the vicinity of each outlet. (a and c) Blood cells moved along both walls and were directed to outlet III. (b) MCF-7 cells moved through the center of the system and were directed to outlet II. Scale bars represent 100 μm.

Table 3 Separation yields of RBC, WBC and MCF-7 using the combination of MOFF and DEP separation

Sample name		RBC	WBC	MCF-7
Recovery	Outlet II	0.76	5.77	75.81[a]
	Outlet I + III	99.24[a]	94.23[a]	24.19
Purity	Outlet II	80.62	3.14	16.24[b]
	Outlet I + III	98.24	1.45	0.31

[a] Final recovery of each cell. 75.81% of MCF-7 cells were isolated using our MOFF-DEP device, while 99.24% of RBCs and 94.23% of WBCs were removed. [b] The final fraction of MCF-7 cells from the separated sample. Since the fraction of MCF-7 at the introduced sample was 0.1%, the enrichment factor was 162.4.

Conclusions

Hydrodynamic and dielectrophoretic separation techniques were shown to be a complementary combination. Both methods are label-free and continuous, and their integration resulted in fast (with respect to flow rate) and efficient performance. We reported a novel method of cell sorting through the combination of MOFF and DEP separation. The serial combination of these two different sorting techniques enabled high-speed continuous flow-through separation, which is not easy to achieve in a microfluidic separation device. We demonstrated its use through the successful separation of MCF-7 cells (a model for circulating tumor cells) from blood. Cells were sorted based first on their size in the MOFF channel and then on their dielectrophoretic properties in the DEP channel. We observed up to 162-fold enrichment of the MCF-7 cells at a 126 μL min^{-1} flow rate. Red and white blood cells were removed with separation efficiencies of 99.24% and 94.23%, respectively. Although our device can handle very high volumetric flow rate, in order to be used in clinical applications, sample concentration would have to be increased to a level approaching that of whole blood. Most continuous flow-through separation techniques currently use diluted blood samples to avoid channel blocking, resulting in a reduced throughput; in contrast, our device showed relatively higher throughput. By adjusting the geometry, arrangement and actuation parameters in the proposed system, we believe our strategy of combing MOFF and DEP could be used to sort a variety of targets with higher throughput, indicating significant potential for many areas of sample preparation in diagnostics and biomedical applications.

Acknowledgements

This research was supported by research programs (grant no. 2009-0072750, 2008-05943) through the National Research Foundation of Korea (NRF). Research facilities were kindly provided by the National Core Research Center (NCRC) for Nanomedical Technology (grant no. R15-2004-024-00000-0) and by the Innovation Cluster for Bio-Fusion Industry of Seoul R&BD program (grant no. 10816).

References

1 K. Pantel, R. Brakenhoff and B. Brandt, *Nat. Rev. Cancer*, 2008, **8**, 329–340.
2 I. Georgakoudi, N. Solban, J. Novak, W. L. Rice, X. Wei, T. Hasan and C. P. Lin, *Cancer Res.*, 2004, **64**, 5044–5047.
3 S. Mocellin, U. Keilholz, C. R. Rossi and D. Nitti, *Trends Mol. Med.*, 2006, **12**, 130–139.
4 S. I. Kim and H.-I. Jung, *J. Breast Cancer*, 2010, **13**, 125–131.
5 S. Nagrath, L. Sequist, S. Maheswaran, D. Bell, D. Irimia, L. Ulkus, M. Smith, E. Kwak, S. Digumarthy and A. Muzikansky, *Nature*, 2007, **450**, 1235–1239.
6 A. Adams, P. Okagbare, J. Feng, M. Hupert, D. Patterson, J. Gottert, R. McCarley, D. Nikitopoulos, M. Murphy and S. Soper, *J. Am. Chem. Soc.*, 2008, **130**, 8633–8641.
7 G. Deng, M. Herrler, D. Burgess, E. Manna, D. Krag and J. Burke, *Breast Cancer Res.*, 2008, **10**, R69.
8 F. F. Becker, X. B. Wang, Y. Huang, R. Pethig, J. Vykoukal and P. R. Gascoyne, *Proc. Natl. Acad. Sci. U. S. A.*, 1995, **92**, 860–864.
9 H. Mohamed, M. Murray, J. N. Turner and M. Caggana, *J. Chromatogr., A*, 2009, **1216**, 8289–8295.
10 K. Han, A. Han and A. Frazier, *Biosens. Bioelectron.*, 2006, **21**, 1907–1914.
11 W. Allard, J. Matera, M. Miller, M. Repollet, M. Connelly, C. Rao, A. Tibbe, J. Uhr and L. Terstappen, *Clin. Cancer Res.*, 2004, **10**, 6897.
12 V. Zieglschmid, C. Hollmann and O. Böcher, *Crit. Rev. Clin. Lab. Sci.*, 2005, **42**, 155–196.
13 H. Kahn, A. Presta, L. Yang, J. Blondal, M. Trudeau, L. Lickley, C. Holloway, D. McCready, D. Maclean and A. Marks, *Breast Cancer Res. Treat.*, 2004, **86**, 237–247.
14 R. T. Krivacic, A. Ladanyi, D. N. Curry, H. B. Hsieh, P. Kuhn, D. E. Bergsrud, J. F. Kepros, T. Barbera, M. Y. Ho, L. B. Chen, R. A. Lerner and R. H. Bruce, *Proc. Natl. Acad. Sci. U. S. A.*, 2004, **101**, 10501–10504.
15 R. Chein, Y. C. Yang and Y. Lin, *Electrophoresis*, 2006, **27**, 640–649.
16 D. Di Carlo, *Lab Chip*, 2009, **9**, 3038–3046.

17 D. Di Carlo, D. Irimia, R. Tompkins and M. Toner, *Proc. Natl. Acad. Sci. U. S. A.*, 2007, **104**, 18892.
18 D. Di Carlo, J. Edd, D. Irimia, R. Tompkins and M. Toner, *Anal. Chem.*, 2008, **80**, 2204.
19 J. Park and H. Jung, *Anal. Chem.*, 2009, **81**, 8280–8288.
20 J. Park, S. Song and H. Jung, *Lab Chip*, 2009, **9**, 939–948.
21 H. Pohl, *Dielectrophoresis: The Behavior of Neutral Matter in Nonuniform Electric Fields*, Cambridge University Press Cambridge, 1978.
22 J. Voldman, *Annu. Rev. Biomed. Eng.*, 2006, **8**, 425.
23 H. Moon, Y. Nam, J. Park and H. Jung, *Environ. Sci. Technol.*, 2009, **43**, 5857.
24 U. Kim and H. Soh, *Lab Chip*, 2009, **9**, 2313–2318.
25 J. Jung, S. I. Han, H. Lee, M. Yoo, and K. H. Han, *The 14th International Conference on Miniaturized Systems for Chemistry and Life Sciences*, Groningen, 2010.
26 A. A. S. Bhagat, H. W. Hou, S. Huang, C. T. Lim, and J. Han, *The 14th International Conference on Miniaturized Systems for Chemistry and Life Sciences*, Groningen, 2010.
27 C. G. Rao, D. Chianese, G. V. Doyle, M. C. Miller, T. Russell, R. A. Sanders, Jr and L. W. Terstappen, *Int. J. Oncol.*, 2005, **27**, 49–57.
28 W. Coleman and G. Tsongalis, *The Molecular Basis of Human Cancer*, Humana Pr Inc, 2002.
29 C. Torres, *Alternative Lithography: Unleashing the Potentials of Nanotechnology*, Springer, New York, 2003.
30 C. Sanders, C. Nelson, M. Hove and G. L. Woods, *Diagn. Microbiol. Infect. Dis.*, 1998, **32**, 111–113.